Forces between a Rigid Probe Particle and a Liquid Interface: Comparison between Experiment and Theory

Sarah A. Nespolo,[†] Derek Y. C. Chan,*,[‡] Franz Grieser,[§]
Patrick G. Hartley,[§,||] and Geoffrey W. Stevens[†]

*Department of Chemical Engineering, Department of Mathematics and Statistics, and
School of Chemistry, Particulate Fluids Processing Centre, The University of Melbourne,
VIC, 3010 Australia*

Forces between a silica colloidal particle probe and an immobilized decane droplet in a range of surfactant (sodium dodecyl sulfate, SDS) solution concentrations have been measured using the atomic force microscope. Independent measurements of the droplet ζ potential, colloidal probe surface potential, contact angle, interfacial tension, and probe radius are used as inputs into the interpretive theory developed by Chan et al. (*J. Colloid Interface Sci.* **2001**, *236*, 141) to provide a quantitative understanding of the measured forces operating at liquid−liquid interfaces. The theory is used to determine the true separation between the solid and the deformable liquid interface. It provides the link between interfacial deformation and disjoining pressure due to electrical double layer and van der Waals interactions in contributing to the observed force in these experiments. Within experimental error, the theory is able to account for the force vs displacement data obtained from atomic force microscopy measurements. It is shown that, in the presence of SDS, the interaction is always repulsive. As a result of the deformation of the droplet shape, forces up to 5 times larger than those observed between solid surfaces are seen. Variations in the interfacial tension of the deformable droplet have the largest effect on the measured forces.

Introduction

The measurement of surface forces has, for many years, been the focus of much interest in the field of colloid and surface science;[2] the long-range interactions between particles controls the stability of a dispersion against coagulation or flocculation. In addition, the rheology of dispersions can also be determined to a large degree by interparticle forces. The interaction of solid colloidal particles with deformable liquid interfaces is of fundamental interest in many technologically important areas such as mineral processing, fluid−fluid processing, and biomedical technologies. For example, a detailed understanding of the surface forces acting between solid−water and oil−water interfaces is critical in order to control the adhesion and transfer of particulate material in aqueous and nonaqueous media.

The measurement of surface forces involving liquid particles is complex due to interfacial fluidity and deformability. It is known that these two features can have significant effects on hydrodynamic interactions and the resulting dynamic properties of such systems,[3−8] which determine the kinetic stability of emulsions against coalescence.[3−5] Interactions involving deformable interfaces are often interpreted in terms of measurable properties such as contact angle, interfacial tension, and electrophoretic mobility. Such measurements alone provide a qualitative correlation with long-range interactions in such systems but do not furnish details about the response of a deformable interface to the force field of an approaching particle or surface.[9]

The surface force apparatus (SFA)[10,11] was originally developed to measure interparticle forces between two molecularly smooth mica surfaces. The SFA has contributed to the understanding of the forces down to separations of molecular scale and their quantitative correlation with surface properties.[12] The development of the atomic force microscope (AFM) has enabled measurement of in situ interaction forces between any kind of surfaces and not just molecularly smooth ones. Ducker et al.[13] first reported the attachment of a colloidal particle, typically 5 μm in diameter, to the AFM cantilever and used this particle to probe surface forces. Although the colloidal probe technique of atomic force microscopy is now a routine method for exploring interfacial phenomena between two solid surfaces,[13,14] precise measurement of such forces when one or both of the particles is deformable has been more elusive.

The first direct measurements of particle-deformable interface interactions were made by Butt.[15] He measured

* Author for correspondence. E-mail: d.chan@unimelb.edu.au.
[†] Department of Chemical Engineering, The University of Melbourne.
[‡] Department of Mathematics and Statistics, The University of Melbourne.
[§] School of Chemistry, The University of Melbourne.
[||] Current address: CSIRO Molecular Science, Clayton South, VIC, 3169, Australia.

(1) Chan, D. Y. C.; Dagastine, R. R.; White, L. R. *J. Colloid Interface Sci.* **2001**, *236*, 141.
(2) Israelachvili, J. N. *Intermolecular and Surface Forces*, 2nd ed.; Academic Press: London, 1991.
(3) *Thin Liquid Films. Fundamentals and Applications*; Ivanov, I. B., Kralchevsky, P. A., Eds.; Marcel Dekker: New York, 1988; Vol. 29.
(4) Ivanov, I. B. *Pure Appl. Chem.* **1980**, *52*, 1241.
(5) Ivanov, I. B.; Dimitrov, D. S.; Somasundaran, P.; Jain, R. K. *Chem. Eng. Sci.* **1985**, *44*, 137.
(6) Traykov, T. T.; Ivanov, I. B. *Int. J. Multiphase Flow* **1977**, *3*, 471.
(7) Zhang, X.; Davis, R. H. *J. Fluid Mech.* **1991**, *230*, 479.

(8) Yiantsios, S. G.; Davis, R. H. *J. Colloid Interface Sci.* **1991**, *144*, 421.
(9) Kelsall, G. H.; Tang, S.; Yurdakul, S.; Smith, A. L. *J. Chem. Soc., Faraday Trans.* **1996**, *92*, 3887.
(10) Israelachvili, J. N.; Adams, G. E. *J. Chem. Soc., Faraday Trans. 1* **1978**, *74*, 975.
(11) Israelachvili, J. N. *Acc. Chem. Res.* **1987**, *20*, 415.
(12) Israelachvili, J. N.; Adams, G. E. *Nature* **1976**, *262*, 775.
(13) Ducker, W. A.; Senden, T. J.; Pashley, R. M. *Nature* **1991**, *353*, 239.
(14) Ducker, W. A.; Senden, T. J.; Pashley, R. M. *Langmuir* **1992**, *8*, 1831.

forces between a silica particle attached to the AFM cantilever and an air bubble anchored to the piezo-driven stage in an aqueous environment. Similar experiments with air bubbles have been reported.[16-22] Measurements of forces between a probe particle and sessile oil drops submerged in water have been reported by Mulvaney et al.,[23] Synder et al.,[24] Hartley et al.,[25] Basu and Sharma,[26] and Aston and Berg.[27,28]

The methodologies for the study of interactions between nondeformable surfaces are well established, and for well-characterized systems, experimental results are in good agreement with theoretical predictions.[29-31] Unfortunately, an interpretation of AFM interparticle-force experiments is not straightforward when the surfaces can deform during interaction. Because of such deformations, the surface shapes and hence the effective interaction areas are not known a priori, but they will vary with surface separation. The other difficulty with measurements involving a deformable surface is the lack of a quantitative theoretical model. Until recently, the interpretation of these measurements requires the additional assumption that the bubble/drop behaves either as an elastic or a nondeformable solid. For instance, the work of Ducker et al.[16] requires the assumption that the air bubble deforms in a linear manner in order to estimate the separation between the two interfaces in AFM force measurements.

To avoid additional assumptions as to how an interface may deform, it is necessary to model surface deformation and surface forces in a consistent way. Miklavcic and co-workers[32-35] have recently addressed the mathematical complexities associated with a deformable fluid interface and a flat solid using the augmented Young–Laplace equation to describe the drop profile evolution in a surface force experiment. This theory has been tested against the work of Horn et al.,[36] who measured surface and hydrodynamic forces between a mercury drop and a flat mica surface, using a modification of the SFA, and showed reasonable agreement between experiment and theory.

Another theoretical model was developed by Bhatt et al.[37] Although they developed a way of comparing experiments to theoretical predictions, they did not give a direct comparison between theory and experimental data.

Aston and Berg[27,28] reported force measurements between a polystyrene particle and a hexadecane droplet at varying salt concentrations and at a single sodium dodecyl sulfate (SDS) concentration. There were two observations that differ from the work reported here. They did not report any engulfment of the colloidal probe by the droplet, which we saw in all of the salt systems without the presence of SDS. They also observed a dependence of their force curves on speed if the piezoelectric stage was driven above 2 μm/s. We do not observe any systematic speed dependence in the range 0.04–3.7 μm/s.

Chan et al.[1] modeled the AFM measurement of forces between a solid colloidal particle probe and a deformable liquid sessile drop on the piezo-driven stage. They developed a theory to relate the observed force to the known displacement of the stage while taking into account deformations of the liquid interface. These experimentally accessible quantities can be modeled in terms of the disjoining pressure, Π, the surface potential of the colloidal probe and the droplet at infinite separation, ψ_{o1}, ψ_{o2}, interfacial tension, γ, Debye length, κ^{-1}, contact angle, θ, particle probe radius, a, and the dielectric and spectroscopic properties of all media. From this theory, it is possible to deduce a quantitative picture of the deformation of the liquid interface as a function of separation.

In this paper, we investigate the force–distance profile for a range of SDS concentrations. We compare our experimental results with theory in some detail. Independent measurements of droplet ζ potential, colloidal probe surface potential, contact angle, interfacial tension, and probe radius are used as inputs into the interpretive theory[1] to provide a quantitative understanding of the measured forces operating at liquid–liquid interfaces. The theory also allows the determination of the true separation between the solid–liquid interface and provides an understanding of the interplay between interfacial deformation and surface forces in this system and known material properties needed to calculated electrical double layer and van der Waals interactions with retardation and salt-screening effects. The picture that emerges has important implications in understanding both emulsion stability and wetting phenomena.

Theory

To understand force measurements involving deformable surfaces, it is necessary to revisit details of the way output from AFM measurements is processed to facilitate comparison with theory. The schematic layout of the AFM apparatus is given in Figure 1a for the case of a colloidal probe particle of radius, a, interacting with a droplet. During force measurements, the decane droplet is driven toward the colloidal probe particle via the piezo displacement, l, of the stage. The force, F, between the particle and the droplet is obtained by monitoring the change in the photodiode voltage that is proportional to the deflection, d, of the cantilever with known spring constant, K_c. The application of Hooke's law gives

$$F = K_c d \tag{1}$$

From the geometry of the apparatus, Figure 1a, the cantilever deflection, d, the distance of closest approach between the particle and the droplet, D_0, and the height of the apex of the drop, z_0, are related by

$$d = l + D_0 + z_0 + 2a - L \tag{2}$$

(15) Butt, H.-J. *J. Colloid Interface Sci.* **1994**, *166*, 109.

(16) Ducker, W. A.; Xu, Z.; Israelachvili, J. N. *Langmuir* **1994**, *10*, 3279.

(17) Fielden, M. L.; Hayes, R. A.; Ralston, J. *Langmuir* **1996**, *12*, 3721.

(18) Preuss, M.; Butt, H.-J. *Langmuir* **1998**, *14*, 3164.

(19) Preuss, M.; Butt, H. J. *Int. J. Mineral. Process.* **1999**, *56*, 99.

(20) Ralston, J.; Fornasiero, D.; Hayes, R. *Int. J. Mineral. Process.* **1999**, *56*, 133.

(21) Ecke, S.; Preuss, M.; Butt, H. J. *J. Adhes. Sci. Technol.* **1999**, *13*, 1181.

(22) Carambassis, A.; Jonker, L. C.; Attard, P.; Rutland, M. W. *Phys. Rev. Lett.* **1998**, *80*, 5357.

(23) Mulvaney, P.; Perera, J. M.; Biggs, S.; Grieser, F.; Stevens, G. W. *J. Colloid Interface Sci.* **1996**, *183*, 614.

(24) Synder, B. A.; Aston, D. E.; Berg, J. C. *Langmuir* **1997**, *13*, 590.

(25) Hartley, P. G.; Grieser, F.; Mulvaney, P.; Stevens, G. W. *Langmuir* **1999**, *15*, 7282.

(26) Basu, S.; Sharma, M. M. *J. Colloid Interface Sci.* **1996**, *181*, 443.

(27) Aston, D. E.; Berg, J. C. *J. Pulp Paper Sci.* **1998**, *24*, 121.

(28) Aston, D. E.; Berg, J. C. *J. Colloid Interface Sci.* **2001**, *235*, 162.

(29) Derjaguin, B. V.; Landau, L. *Acta Physicochem.* **1941**, *14*, 633.

(30) Verwey, E. J. W.; Overbeek, J. T. G. *Theory and Stability of Lyphobic Colloids*; Elsevier: Amsterdam, 1948.

(31) Hunter, R. J. *Foundations of Colloid Science*; Oxford Science Publishers: Oxford, England, 1989; Vol. 1.

(32) Miklavcic, S. J.; Horn, R. G.; Bachmann, D. J. *J. Phys. Chem.* **1995**, *99*, 16357.

(33) Bachmann, D. J.; Miklavcic, S. J. *Langmuir* **1996**, *12*, 4197.

(34) Miklavcic, S. *J. Phys. Rev. E: Stat. Phys., Plasmas* **1996**, *54*.

(35) Miklavcic, S. J.; Attard, P. *J. Phys. A: Math. Gen.* **2001**, *34*, 7849.

(36) Horn, R. G.; Bachmann, D. J.; Connor, J. N.; Miklavcic, S. J. *J. Phys.: Condens. Matter* **1996**, *8*, 9483.

(37) Bhatt, D.; Newman, J.; Radke, C. J. *Langmuir* **2001**, *17*, 116.

Figure 1. (a) Schematic diagram of the interaction between a colloidal probe particle attached to the AFM cantilever and a deformable droplet. The undeformed (original) shape is represented by the broken line. (b) Schematic illustration of the variation of the cantilever deflection, d, with the displacement, l, of the stage for repulsive interactions.

The schematic variation of cantilever deflection, d, with the displacement, l for repulsive interactions is illustrated in Figure 1b.

If the droplet is a rigid body (where z_o is a constant), a plot of d vs l exhibits a linear compliance region (see Figure 1b) in which the distance of closest approach, D_o, attains some constant value D_w that is independent of l and may be regarded as the "zero" separation. By fitting a straight line to this linear region

$$y \equiv ml + c = l + (D_w + z_o + 2a - L) \qquad (3)$$

where m is equal to unity for a rigid system, we can deduce the separation between two interacting rigid bodies by subtracting eq 3 from eq 2 to give

$$D_o - D_w = d - y \quad \text{(droplet as a rigid body)} \qquad (4)$$

If the droplet is treated as an effective linearly elastic body with an elastic constant, K_d, the force will also be proportional to the deformation of the droplet

$$F = K_d(z_o^\infty - z_o) \qquad (5)$$

where z_o^∞ is the height of the apex of the undistorted interface. Combining eqs 2 and 5, we have

$$d = \frac{K_d}{K_d + K_c} (l + D_o + z_o^\infty + 2a - L) \qquad (6)$$

and the straight line fit to the linear compliance region is

$$y \equiv ml + c = \frac{K_d}{K_d + K_c} (l + D_w + z_o^\infty + 2a - L) \quad (7)$$

where the slope of this line, $m = K_d/(K_d + K_c)$, provides an estimate of the effective elastic constant of the droplet. The separation between the particle and the droplet can be obtained from

$$D_o - D_w = \frac{K_d + K_c}{K_d} (d - y)$$

$$\text{(droplet as an elastic body)} \qquad (8)$$

which again facilitates the extraction of force vs separation data from AFM measurements.

When the droplet deformation is governed by interfacial tension and surface forces, it is necessary to know how the droplet profile and, in particular, the droplet height, z_o, varies with separation, D_o, in a self-consistent way. If the disjoining pressure between the particle and the droplet interface can be specified, the droplet shape and the height, z_o, can be calculated in terms of the separation, D_o, via the Young−Laplace equation augmented by the specified disjoining pressure. Thus, for deformable droplets, we compare experimental force data presented in the form

$$[F_{\text{expt}} \equiv] \ K_c d \quad \text{vs} \quad \Delta(d - l)_{\text{expt}} \ [\equiv \Delta(D_o + z_o)_{\text{expt}}] \qquad (9)$$

with the theory given in the form

$$F_{\text{theory}} \text{ vs } \Delta X_{\text{theory}} \ [\equiv \ \Delta(D_o + z_o)_{\text{theory}}] \qquad (10)$$

The arbitrary constant in the abscissa allows a one-off horizontal relative translation of the experimental and theoretical force curves to bring them into agreement. This analysis is very similar to the case of a rigid droplet except that because the droplet height, z_o, is a function of separation, the quantity $\Delta(d - l)$ is no longer the change in separation, ΔD_o, between the particle and the droplet surface.

For the experimental system we consider here, there are large differences between the characteristic lengths of the system: the separation, $D_o \sim 100$ nm, the particle radius, $a \sim 2\ \mu$m, and the undistorted radius of curvature of the droplet, $R_o \sim 1$ mm. For such small oil-in-water droplets, gravitational effects are negligible. A detailed theoretical analysis of the problem in this regime has been given elsewhere[1]. The distance between the particle and the fluid interface, D (see Figure 1a), was obtained in terms of the solution of the differential equation

$$\frac{d^2 D(t)}{dt^2} + \frac{1}{t}\frac{dD(t)}{dt} = D_o\left(2\left(1 + \frac{a}{R_o}\right)\frac{a\Pi(D(t))}{\gamma}\right) \quad (11)$$

where $t = r/(a\ D_o)^{1/2}$ is an order 1 scaled variable over which the interface is deformed as a result of surface forces; $\Pi(D)$ is the disjoining pressure that varies with separation D, and γ is the interfacial tension of the droplet. The boundary conditions at $t = 0$ are $D = D_o$ and $dD(t)/dt = 0$. The solution of eq 11 is matched to the solution of the Young−Laplace equation that determines the drop shape in the region where effects due to surface forces may be omitted. Although this outer region of the dropet does not experience any direct surface force due to the colloid probe, its shape is nonetheless deformed from that of the isolated droplet because of the conservation of the droplet volume.

The final expression for $\Delta X(D_o)$ is given by

$$\Delta X(D_o) = D_o + H(D_o) + G(D_o)\left\{\log\left(\frac{(aD_o)^{1/2}}{2R_o}\right) + P(\theta_c)\right\} \quad (12)$$

where

$$G(D_o) = \frac{aD_o}{\gamma} \int_0^\infty dt\, t\Pi(D(t)) \quad (13)$$

$$H(D_o) = \frac{aD_o}{\gamma} \int_0^\infty dt\, t(\log t)\Pi(D(t)) \quad (14)$$

and the total force between the particle and the droplet is

$$F(D_o) = 2\pi\gamma G(D_o) \quad (15)$$

The quantity $P(\theta_c)$ depends on the equilibrium contact angle, θ_c, measured through the oil phase, at the oil−water−piezo stage three-phase contact line. The function $P(\theta_c)$ depends on assumptions about the behavior of this three-phase contact line during particle−droplet interaction. Two plausible limits of behavior are either the contact line remains immobile during interaction (and the contact angle will therefore change) or the contact angle will remain constant at the equilibrium contact angle, θ_c (and the three phase contact line will move). In these two limits, $P(\theta_c)$ will be given by[38]

$$P(\theta_c) = 1 + \frac{1}{2}\log\left(\frac{1 + \cos\theta_c}{1 - \cos\theta_c}\right) \text{ (immobile contact line)}$$
$$(16)$$

or

$$P(\theta_c) = \left(\frac{1 + \cos\theta_c}{1 + 2\cos\theta_c}\right) + \frac{1}{2}\log\left(\frac{1 + \cos\theta_c}{1 - \cos\theta_c}\right)$$
$$\text{(constant contact angle)} \quad (17)$$

If during droplet deformation, the droplet and the substrate can maintain equilibrium conditions at the three phase contact line, then the constant contact angle condition will apply and eq 17 should be used. However, if the three phase contact line is pinned by surface roughness or there is contact angle hysteresis effect, eq 16 is more appropriate. However, the contact angles encounted in the present experiments are close to 90° so the difference between eq 16 and eq 17 is not large.

Thus, the task is to solve eq 11 numerically for a given model of the disjoining pressure, $\Pi(D)$, and then use the result in eqs 12−17 to generate theoretical results in the form of eq 10 suitable for comparison with experimental data in the form of eq 9. This provides a test of the parameters in the model for the disjoining pressure.

If the disjoining pressure, $\Pi(D)$, is made up of the familiar electrical double layer repulsion and van der Waals attraction, there will be a maximum in $\Pi(D)$ (see Figure 2, $\Pi(D) > 0$ denotes repulsive interactions). An approximate criterion for stability is as follows. If this maximum is less than $2\gamma(1/a + 1/R_o)$ (curve U in Figure 2), the particle probe will be engulfed by the droplet at sufficiently small separations and the particle−droplet interaction will be unstable. However, if the maximum in

(38) The original expression for $P(\theta_c)$ in Chan et al.[1] for the immobile contact line case is incorrect.
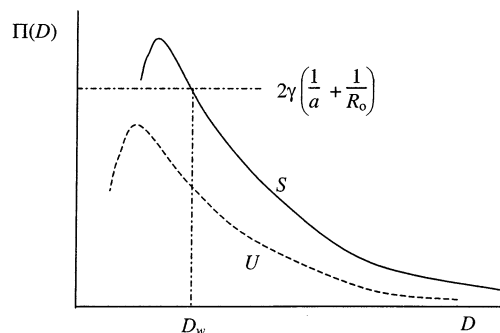
Figure 2. Schematic forms of the maxima in the disjoining pressure, $\Pi(D)$, relative to the Laplace pressure, $2\gamma(1/a + 1/R_o)$, and the location of the position, D_w. ($\Pi(D) > 0$ corresponds to repulsion.)

$\Pi(D)$ is greater than $2\gamma(1/a + 1/R_o)$ (curve S in Figure 2), the disjoining pressure will be sufficient to balance the Laplace pressure of the curved droplet interface that will be wrapped around the particle, and the particle−droplet interaction is stable. Strictly the stability condition requires that the magnitude of the slope of $\Pi(D)$ be sufficiently large at D_w, defined by the equation

$$\Pi(D_w) = 2\gamma\left(\frac{1}{a} + \frac{1}{R_o}\right) \quad (18)$$

so that the distance of closest approach between the particle and the droplet interface will always be larger than D_w (see later).

At large separations where the deformation of the droplet interface is small, an approximate analytical expression for the force is

$$\frac{F(D_o)}{a} \approx \frac{2\pi E(D_o)}{1 - \frac{2a}{\gamma}\Pi(D_o)} \quad (19)$$

where $E(D_o)$ is the interaction free energy per unit area between the solid particle and the droplet under the assumption that they are both parallel flat surfaces. The disjoining pressure $\Pi(D_o)$ and $E(D_o)$ are related by

$$\Pi(D_o) = -\frac{dE(D_o)}{dD_o} \quad (20)$$

The numerator on the right-hand side of eq 19 is the familiar Derjaguin approximation assuming that the droplet has a fixed (nondeformable) radius of curvature, $R_o \gg a$. The denominator can be interpreted as a factor that expresses the increase in the effective area of interaction due to deformations of the droplet interface. Clearly eq 19 can only be afforded this physical interpretation when

$$D_o \gg D_w \text{ or } \Pi(D_o) \ll 2\gamma\left(\frac{1}{a} + \frac{1}{R_o}\right)$$

In the present theoretical model, we have not included the possibility of dynamical effects due for example to the relative viscosities of the electrolyte and the droplet and the rate of approach of the droplet toward the colloid probe. This is because within the range of AFM piezo scan rates that we employed, the forces we measured are independent of the scan rate. We therefore take this as evidence that, within the range of scan rates, the system behaves as

though it is able to maintain equilibrium throughout the measurement.

Experimental Details

Materials. The anionic surfactant, sodium dodecyl sulfate, SDS, was obtained from BDH Laboratory Supplies. Sample purity was verified by using solution conductivity to measure the critical micelle concentration (cmc) as 7.9 mM, which is in good agreement with literature values.[39] Electrolytes were analytical grade reagents and were used without further purification. AR grade *n*-decane used in these experiments was from Aldrich and was used without further purification. Melinex polymer film was used for the immobilization of the *n*-decane droplets. Melinex film is a pure, semicrystalline PET film, not containing any filler, and does not have any coating layers on either surface.

All samples were prepared using Milli-Q water. All glassware was cleaned by soaking in 10% nitric acid, then by sonication for 1 h in a 1% RBS detergent (Pierce Chemicals)/20% ethanol solution, followed by extensive rinsing with Milli-Q water prior to drying in a laminar flow clean cabinet.

The colloidal silica used as a spherical probe for AFM force measurements was obtained from Allied Signal, prepared by a modified Stöber process, with a diameter range of 4−6 μm.[40] Electrokinetic properties of such silica particles were studied in detail by Hartley et al.[41] Gold-coated silicon nitride cantilevers used in the AFM experiments were obtained in wafer form from Digital Instruments (Santa Barbara, CA). The 24 h curing Araldite epoxy resin used to attach colloidal probes to AFM cantilevers was obtained from Selleys Chemical Co., Padstow, N.S.W., Australia, 2211.

Methods. A Digital Instruments (Santa Barbara, CA) Nanoscope IIIa AFM was used to measure forces between colloidal silica and an *n*-decane, oil droplet. The size of the colloidal silica was determined optically and the error in the measurement was 10%. Experimental details are described in detail elsewhere.[25]

Interfacial tension data were obtained using a First Ten Angstroms, FTÅ200 pendant droplet instrument. All measurements were performed at 25.0 ± 0.1 °C. Images were obtained at 2 frames per second for a period of 60 s.

Contact angle data were obtained using a DataPhysics OCA20 instrument. All measurements were performed at 25.0 ± 0.1 °C.

The determination of the ζ potential on the *n*-decane droplets in the presence of SDS is described in detail elsewhere.[42]

Results and Discussion

From a given form of the disjoining pressure, the force, $F(X)$, can be calculated as a function of the droplet displacement, ΔX, as outlined in the Theory section.[1] In this calculation, the experimental parameters − surface potentials at infinite separation, ψ_{o1}, ψ_{o2}, interfacial tension, γ, Debye length, κ^{-1}, contact angle, θ, droplet radius, R_o, and probe radius, a − are required inputs. The following section describes the independent experimental determination of these parameters under conditions as close as possible to that of the AFM measurements.

Determination of the ζ Potential of the *n*-Decane Droplets. Electrophoretic mobilities of SDS stabilized decane droplets were interpreted in terms of ζ-potentials with the aid of light scattering and SDS surface excess measurements.[42] Depending on whether one assumes the droplet behaves hydrodynamically as a solid particle or as a liquid particle, each measured electrophoretic mobility value can correspond to up to four possible ζ-potentials, as opposed to at most two possibilities for solid particles.[43,44] The combined results from static and dynamic

light scattering and SDS surface excess measurements were consistent with the interpretation that the droplets behaved hydrodynamically and electrokinetically as solid particles. The ζ-potentials for the droplets stabilized with SDS concentrations between 0.01 and 1 mM were found to be between −100 and −125 mV.[42] Since the dependence of the ζ potential on bulk SDS concentration was minimal, the ζ potential for 10 mM SDS, which has not been experimentally determined, is assumed to be between −100 and −125 mV. In this study, we have equated these measurements of ζ potential to the surface potential, ψ_o, of the droplet, an assumption that has been shown to be justified in force measurements, including involving even dissimilar solid surfaces.[49]

Determination of the Surface Potential of the Silica Colloidal Probe. Hartley et al.[41] used electrokinetic and direct force measurements to determine the ζ-potentials of silica in dilute electrolyte solutions as a function of pH. They found for a solution of 10^{-3} M NaNO$_3$, pH 6, ζ-potentials derived from streaming potential measurements, electrophoresis studies of silica colloids, as well as from fitting the diffuse double layer potentials to AFM force−distance data, resulted in an average ζ-potential of −50 mV. There was significant experimental variation in all these measurements, both, in the individual experiments and in the comparison between methods. An error of ±20 mV could be considered a reasonable error range for the surface potential of the silica probe in the present measurements. Since SDS is well-known not to adsorb to silica, this ζ-potential has been used for the silica surface potential value in all of the SDS solutions, since the background electrolyte used in these measurements was 10^{-3} M NaNO$_3$.

Determination of Interfacial Tension. AR grade decane-aqueous interfacial tension data were obtained using a DataPhysics OCA20 pendant droplet instrument. All measurements were performed at 25.0 ± 0.1 °C. The static or initial interfacial tension value was obtained by recording images at 2 frames per second for a period of 60 s. If any surface-active contaminants were present, then over time, these will reduce the interfacial tension. With no SDS present, the interfacial tension took 4 h to reach equilibrium. As surfactant was added, the time needed to equilibrate decreased. In Figure 3, we summarize the time dependence behavior of such interfacial data.

Goebel and Lunkenheimer also observed similar time dependence in interfacial tension measurements. They found that with purification of the decane, the interfacial tension remained constant over time. They concluded that the time dependence of the interfacial tension was due to the amphiphilic character of surface-active impurities in commercially available oils.[45] This interpretation is consistent with the decrease in the time to reach equilibrium with increasing SDS concentration. At high SDS concentrations, it is the adsorption of SDS at the interface rather than that of trace impurities that determines the equilibrium interfacial tension. In the analysis of force measurements in the presence of surfactants, the equi-

(39) Rosen, M. J. *Surfactants and Interfacial Phenomena*; John Wiley & Sons: New York, 1974.

(40) Barder, T. J.; Dubois, P. D. U.S. Patent 1991; Vol. 983.

(41) Hartley, P. G.; Larson, I.; Scales, P. J. *Langmuir* **1997**, *13*, 2207.

(42) Nespolo, S. A.; Bevan, M. A.; Chan, D. Y. C.; Grieser, F.; Stevens, G. W. *Langmuir* **2001**, *17*, 7210.

(43) O'Brien, R.; White, L. R. J. *Chem. Soc., Faraday Trans. 2* **1978**, *74*, 1607.

(44) Ohshima, H.; Healy, T. W.; White, L. R. *J. Chem. Soc., Faraday Trans. 2* **1984**, *80*, 1643.

(45) Goebel, A.; Lunkenheimer, K. *Langmuir* **1997**, *13*, 369.

(46) Cleveland, J. P.; Manne, S.; Bocek, D.; Hansma, P. K. *Rev. Sci. Instrum.* **1993**, *64*, 403.

(47) Sader, J. E.; Larson, I.; Mulvaney, P.; White, L. R. *Rev. Sci. Instrum.* **1995**, *66*, 3789.

(48) Hough, D. B.; White, L. R. *Adv. Colloid Interface Sci.* **1980**, *14*, 3.

(49) Larson, I.; Drummond, C. J.; Chan, D. Y. C.; Grieser, F. *Langmuir* **1997**, *13*, 2109.

Figure 3. Interfacial tension data for a decane droplet in 10^{-3} M $NaNO_3$, pH 5.6, at different concentrations of SDS as a function of time from pendant droplet measurements at 298 K. Error bars are displayed for the individual runs.

librium values of the interfacial tensions were used since force measurements were performed over a time scale similar to that required for equilibration of the oil droplet.

Measured initial and equilibrium interfacial tensions of the water-decane interface for various SDS concentrations are given in Table 1.

Determination of Other Parameters. Contact angles were obtained using a DataPhysics OCA20 instrument.

Table 1. Initial and Equilibrium Interfacial Tension Data from Pendant Droplet Measurements at 298 K for Varying Bulk SDS Concentrations

[SDS] (M)	interfacial tension (mN/m)	
	initial, γ^{init}	equilibrium, γ^{eqm}
0	52.3 ± 1.0	48.5 ± 1.0
10^{-5}	48.7 ± 1.0	39.1 ± 1.0
10^{-4}	45.9 ± 1.0	39.1 ± 1.0
10^{-3}	33.4 ± 0.8	26.5 ± 0.8
10^{-2}	8.6 ± 0.5	8.6 ± 0.5

All measurements were performed at 25.0 ± 0.1 °C. Unlike the interfacial tension data, contact angle data were not observed over time unlike the interfacial tension data since a small change in the contact angle would have little effect on the theoretical curves.

The radius of the colloidal silica and the decane droplet were determined optically and the error in the measurement was $\pm 10\%$.

Errors in the Force Data. There are three sources of error in the force measurements. These are the variations between atomic force microscope scans, uncertainties in the spring constants of the cantilevers, and errors in determining the radius of the colloidal silica sphere probe.

Force measurements were conducted with the colloidal probe positioned above the apex of the droplet. No observable differences were evident when the position of the probe was displaced one probe radius from the apparent apex of the droplet. The decane droplet is driven
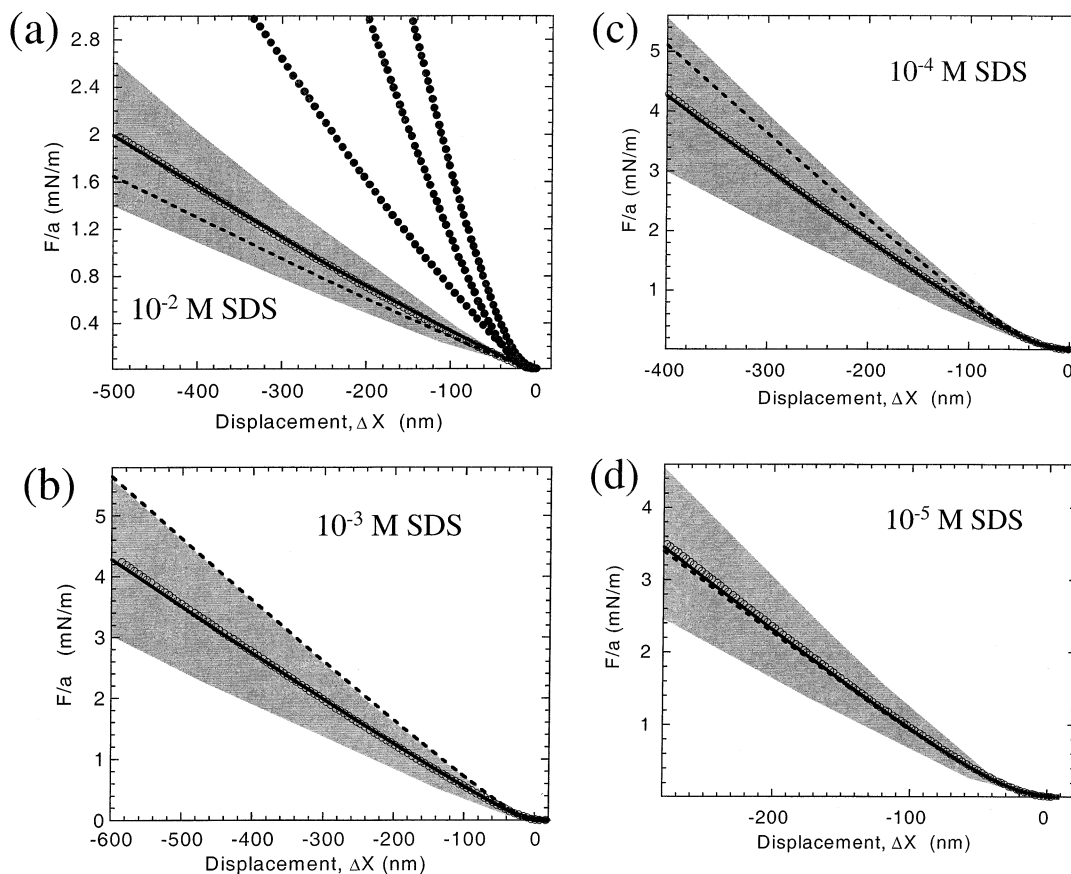
Figure 4. Force divided by probe radius vs displacement, $\Delta X = \Delta(d - l)$, for a silica colloidal probe approaching an n-decane/water interface in (a) 10^{-2} M SDS, (b) 10^{-3} M SDS, (c) 10^{-4} M SDS, and (d) 10^{-5} M SDS, all with 10^{-3} M $NaNO_3$ background electrolyte. Open symbols are the experimental force measurements. Dotted lines are theoretical calculations using experimentally determined parameters reported in Table 2 for a fixed contact line droplet. Solid lines are obtained by using the interfacial tension as an adjustable parameter. (See Table 3.) Filled symbols are the experimental force measurements for 10^{-3} M, 10^{-4} M, and 10^{-5} M SDS, with 10^{-3} M $NaNO_3$ background electrolyte as displayed in parts b–d. The shaded area represents the error ($\sim 30\%$) associated with the force measurements.

Table 2. Experimentally Determined Surface Potentials, Interfacial Tension and Contact Angle for Various Surfactant Solutions at 298 K

solution	surface potential of silica, ψ_{o1} (mV)	surface potential of n-decane, ψ_{o2} (mV)	equilibrium interfacial tension, γ^{eqm} (mN/m)	contact angle, θ, through decane/aqueous/Melinex (deg)	Debye length, κ^{-1}, nm
10^{-5} M SDS, 10^{-3} M NaNO$_3$	−50	−100	39.1	102	9.54
10^{-4} M SDS, 10^{-3} M NaNO$_3$	−50	−100	39.1	94	9.14
10^{-3} M SDS, 10^{-3} M NaNO$_3$	−50	−100	26.5	102	6.78
10^{-2} M SDS, 10^{-3} M NaNO$_3$	−50	−100	8.6	92	2.92

Table 3. Equilibrium and Optimum Fitted Interfacial Tensions for n-decane/SDS^a

solution	interfacial tension (mN/m)	
	equilibrium	fitted
10^{-5} M SDS + 10^{-3} M NaNO$_3$	39.1	38.5−40.0
10^{-4} M SDS + 10^{-3} M NaNO$_3$	39.1	30.5−31.0
10^{-3} M SDS + 10^{-3} M NaNO$_3$	26.5	19.0−19.2
10^{-2} M SDS + 10^{-3} M NaNO$_3$	8.6	9.8−10.2

^{a} The lower limit for the optimum fitted interfacial tensions is for the immobile contact line case (refer to eq 16), and the higher limit is for the constant contact angle case (refer to eq 17).

toward the particle probe at speeds in the range 0.04−3.7 μm/s, no systematic variations of the force were evident within this speed range. Between runs, there is a ±10% variation in the force−displacement data.

The spring constants of the AFM cantilevers used in the experiments were ascertained by selecting several cantilevers from different regions of the cantilever wafer and measuring the spring constants using the method of Cleveland et al.[46] This method relies on monitoring the shifts in resonance frequency as a function of known attached masses to the cantilever. The nondestructive method developed by Sader et al.[47] was also used to determine the spring constants of the other tips on the cantilever wafer. This method relies solely on the determination of the unloaded resonant frequency of the cantilever combined with knowledge of its density or mass and its dimensions. The variability of spring constants determined by these two methods was ±10% across the wafer.

The error associated with the measurement of the radius of the silica sphere, was ±10% as mentioned previously. The cumulative error of ±30% from all sources is indicated by the shaded gray region in the results for the force in Figure 4.

Comparison between Experimental Data and Theory. As described in the Theory section, experimental force data were plotted as a function of the displacement, $\Delta(d - l)$: F_{expt} vs $\Delta(d - l)_{expt}$

Data from the atomic force microscope are recorded as cantilever deflection in volts vs piezo displacement in nm. The conversion of cantilever deflection, d, from voltage to nm is achieved by calibrating the constant compliance slope on a rigid portion of the substrate.

Theory[1] is used to relate the force between a rigid probe particle and a deformable liquid interface due to the disjoining pressure between the solid−liquid and liquid−liquid interface. The electrical double layer component of the disjoining pressure depends on the surface potentials of the probe and droplet at infinite separation, ψ_{1o}, ψ_{2o}, Debye length, κ^{-1}, contact angle, θ, probe radius, a, droplet radius, R_o, and interfacial tension, γ. These are determined by independent experiments as discussed earlier, and their values are given in Table 2. Dielectric and spectroscopic data needed to calculate the van der Waals component of the disjoining pressure are taken from the literature.[48] For all solutions, the probe radius, a, is 2.16 μm, and the
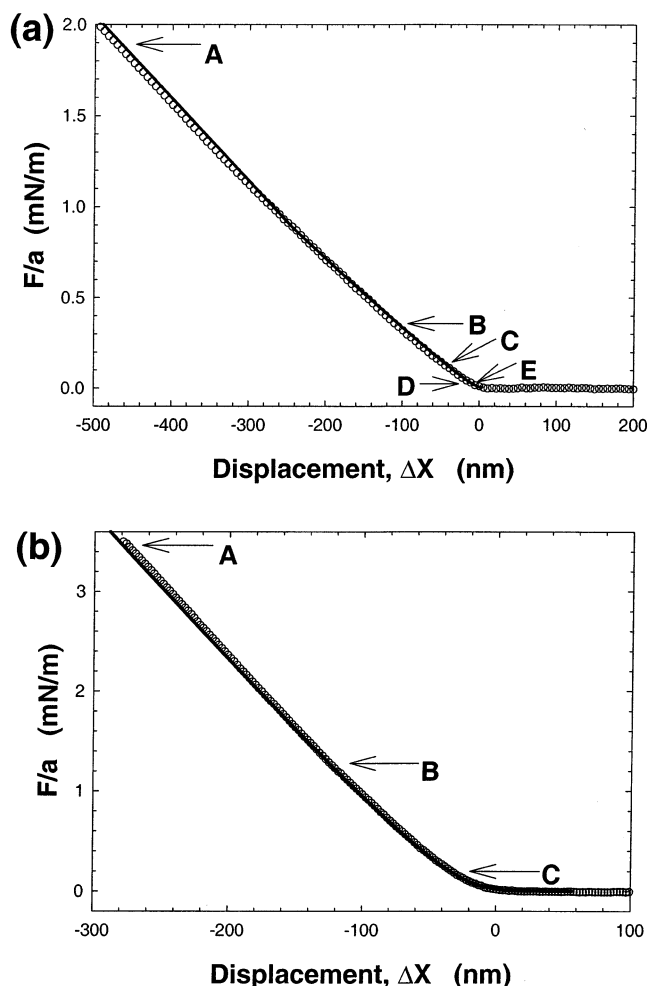
Figure 5. (a) Normalized force, F/a, vs displacement for 10^{-2} M SDS, 10^{-3} M NaNO$_3$. Experimental force measurements are shown in open symbols. The solid line represents results of the theoretical calculation using $\psi_{o1} = -50$ mV, $\psi_{o2} = -100$ mV, $\gamma^{fitted} = 9.8$ mN/m, $R_o = 0.5$ mm, $a = 2.16$ μm, and $\kappa^{-1} = 2.92$ nm. Key: (A) $F/a = 1.9$ mN/m where $D_o = 11.8$ nm; (B) $F/a = 0.37$ mN/m where $D_o = 12.5$ nm; (C) $F/a = 0.10$ mN/m where $D_o = 14.5$ nm; (D) $F/a = 0.02$ mN/m where $D_o = 19.0$ nm,; (E) $F/a = 0.00$ mN/m where $D_o = 25.0$ nm. (b) Normalized force, F/a, vs displacement for 10^{-5} M SDS, 10^{-3} M NaNO$_3$. Experimental force measurements are shown in open symbols. The solid line represents results of the theoretical calculation using $\psi_{o1} = -50$ mV, $\psi_{o2} = -100$ mV, $\gamma^{fitted} = 38.5$ mN/m, $R_o = 0.5$ mm, $a = 2.16$ μm, and $\kappa^{-1} = 9.54$ nm. Key: (A) $F/a = 3.5$ mN/m where $D_o = 8.5$ nm; (B) $F/a = 1.3$ mN/m where $D_o = 13.0$ nm; (C) $F/a = 0.02$ mN/m where $D_o = 28.0$ nm.

droplet radius, R_o, is 0.5 mm. While all these parameters have experimental uncertainties, it was found the portion of the force vs displacement curves, $F/a > 1$ mN/m can only be influenced by variations in the interfacial tension. Variations of other parameters such as the surface potentials and contact angles within experimental uncertainties have little effect at high forces. However, the
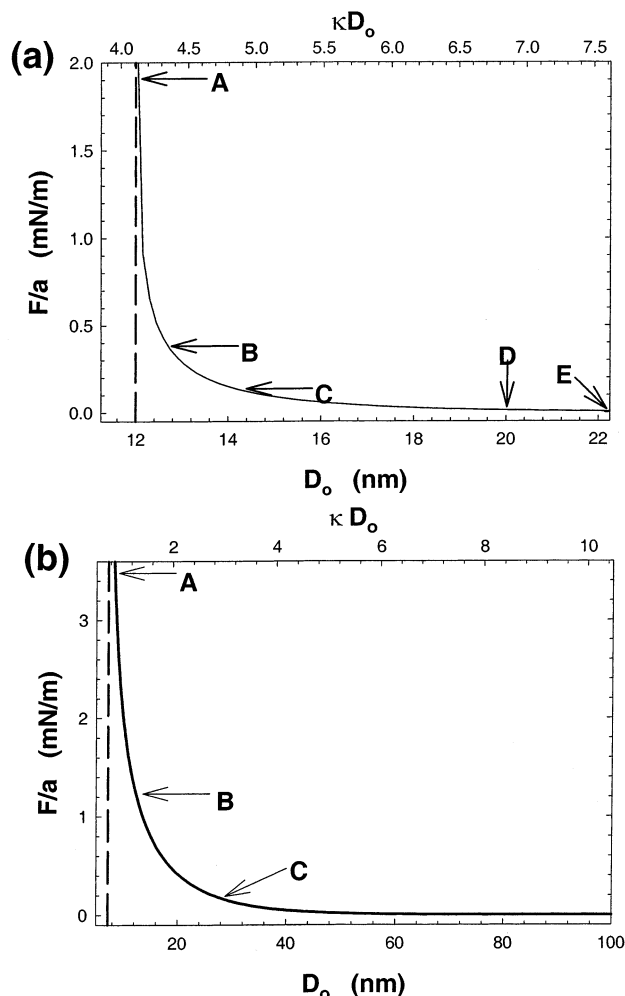
Figure 6. (a) Normalized force, F/a, vs separation between the particle and the droplet, D_o, for 10^{-2} M SDS, 10^{-3} M NaNO$_3$, corresponding to the theoretical results in Figure 5a obtained using $\psi_{o1} = -50$ mV, $\psi_{o2} = -100$ mV, $\gamma^{\text{fitted}} = 9.8$ mN/m, R_o = 0.5 mm, a = 2.16 μm and $\kappa^{-1} = 2.92$ nm. The minimum separation, $D_o = D_w = 12.0$ nm is indicated by the dashed line. (b) Normalized force, F/a, vs separation between the particle and the droplet, D_o, for 10^{-5} M SDS, 10^{-3} M NaNO$_3$, corresponding to the theoretical results in Figure 5b obtained using $\psi_{o1} = -50$ mV, $\psi_{o2} = -100$ mV, $\gamma^{\text{fitted}} = 38.5$ mN/m, R_o = 0.5 mm, $a = 2.16$ μm and $\kappa^{-1} = 9.54$ nm. The minimum separation, $D_o = D_w = 7.4$ nm is indicated by the dashed line.

Table 4. Minimum Separation Determined Theoretically[a]

	minimum separation, D_w (nm)	
solution	equilibrium	fitted
10^{-5} M SDS + 10^{-3} M NaNO$_3$	7.3	7.4
10^{-4} M SDS + 10^{-3} M NaNO$_3$	7.4	8.8
10^{-3} M SDS + 10^{-3} M NaNO$_3$	10.1	12.0
10^{-2} M SDS + 10^{-3} M NaNO$_3$	12.4	12.0

[a] Calculation uses the immobile contact line case; refer to eq 16.

segment of the force curve for $F/a < 1$ mN/m can be fitted equally well by different combinations of the silica and decane surface potentials within the acceptable experimental ranges of these parameters. The results in Figure 4 have been fitted with parameter values given in Table 2, which are mean experimental values that have been determined independently.

Comparison between theory and experiment for the force divided by probe radius, F/a, vs displacement, $\Delta X = \Delta(d - l)$, for a silica colloidal probe approaching an n-decane
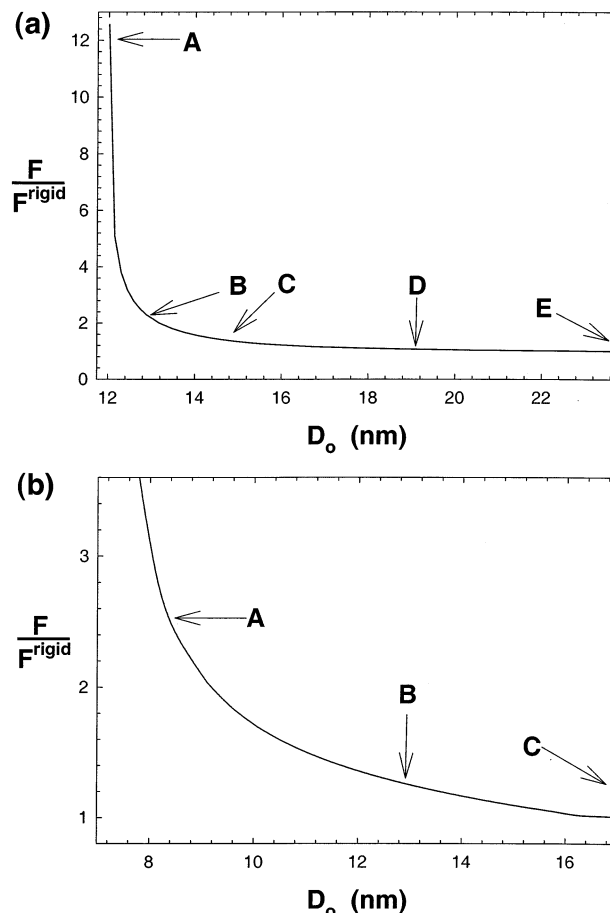
Figure 7. (a) F/F^{rigid} vs separation between the particle and the droplet, D_o for 10^{-2} M SDS, 10^{-3} M NaNO$_3$. The theoretical calculation was performed using $\psi_{o1} = -100$ mV, $\psi_{o2} = -50$ mV, $R_o = 0.5$ mm, $a = 2.16$ μm, and $\kappa^{-1} = 2.92$ nm. For F, $\gamma^{\text{fitted}} = 9.8$ mN/m, for F, $\gamma \to \infty$ mN/m. The minimum separation was $D_w = 12.0$ nm. (b) F/F^{rigid} vs separation between the particle and the droplet, D_o, for 10^{-5} M SDS, 10^{-3} M NaNO$_3$. The theoretical calculation was performed using $\psi_{o1} = -100$ mV, $\psi_{o2} = -50$ mV, $R_o = 0.5$ mm, $a = 2.16$ μm, and $\kappa^{-1} = 2.92$ nm. For F, $\gamma^{\text{fitted}} = 38.5$ mN/m; for F, $\gamma \to \infty$ mN/m. The minimum separation, was $D_w = 7.4$ nm.

interface in 10^{-3} M NaNO$_3$, at different concentrations of SDS are shown in Figure 4. The disjoining pressure is taken to be due to an electrical double layer interaction calculated using the nonlinear Poisson–Boltzmann theory with constant surface charge boundary conditions and a van der Waals force calculated using the full Lifshitz theory that takes into consideration retardation effects and salt effects in the zero frequency term. The open symbols are the experimentally determined force measurements. The dotted lines denote theoretical calculations using experimentally determined parameters reported in Table 2. The solid lines denote theoretical calculations using experimentally determined parameters except that the interfacial tension is varied to fit experimental data. The shaded area represents the estimated error associated with the force measurements as described previously, which can be up to ±30%.

To facilitate comparison across different SDS concentrations, the force curves for 10^{-3} M, 10^{-4} M, and 10^{-5} M SDS are also included in Figure 4a. It is evident that the slopes of these curves correlate with interfacial tension as expected from theory.[1] In all cases presented here, the particle probe–droplet interaction is stable and repulsive at all separations. The range of travel of the piezoelectric
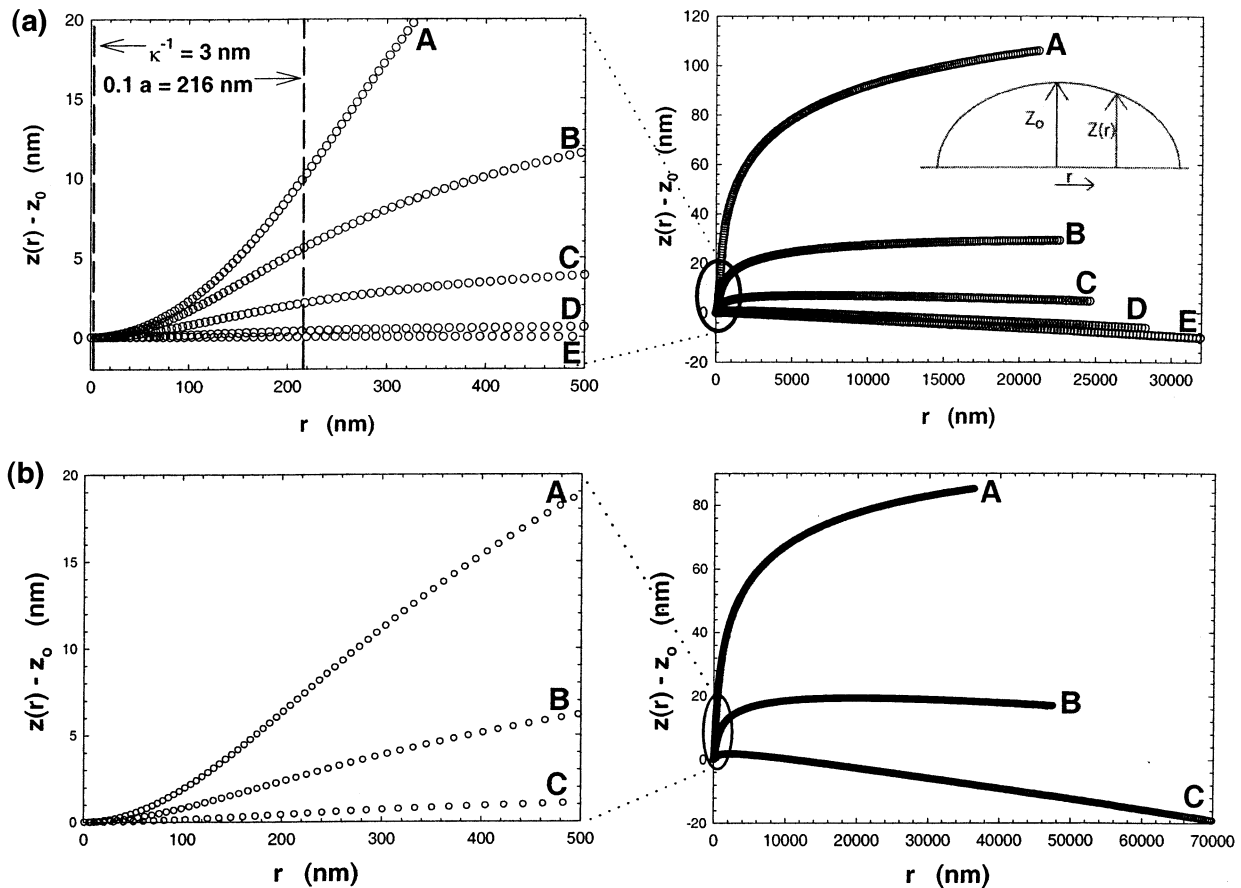
Figure 8. (a) Plot of $z(r) - z_0$ vs r. 10^{-2} M SDS, 10^{-3} M NaNO$_3$. The theoretical calculation using $\psi_{o1} = -50$ mV, $\psi_{o2} = -100$ mV, $\gamma^{\text{fitted}} = 9.8$ N/m, $R_o = 0.5$ mm, $a = 2.16$ μm, $\theta = 92°$, and $\kappa^{-1} = 2.92$ nm. A, B, C, D, E refer to Figure 6a. (b) Plot of $z(r)$-z_0 vs r. 10^{-5} M SDS, 10^{-3} M NaNO$_3$. The theoretical calculation using $\psi_{o1} = $ -50 mV, $\psi_{o2} = -100$ mV, $\gamma^{\text{fitted}} = 38.5$ mN/m, $R_o = 0.5$ mm, $a = 2.16$ μm, $\theta = 102°$, and $\kappa^{-1} = 9.54$ nm. For A–C, refer to Figure 6b.

stage on the AFM is the limiting factor in exploring the range of force values in these measurements.

Using the independently determined physical parameters as input; the theoretical curves fall within experimental uncertainties of force measurements. However, the agreement between theory and experiment for the region $F/a > 1$ mN/m can be improved if the interfacial tension is used as an adjustable parameter. Variations of other parameters such as surface potentials and contact angle within their accepted experimental uncertainty range has little effect for the region $F/a > 1$ mN/m. Modification of the interfacial tension, resulted in fitted interfacial tensions given in Table 3. These fitted interfacial tensions produce the solid lines in Figure 4. For example in the case of the 10^{-3} M SDS solution, with 10^{-3} M NaNO$_3$, the equilibrium interfacial tension is 26.5 mN/m, while the fitted interfacial tension is about 19 mN/m. The difference of around 7 mN/m corresponds to a reduction in the area per surfactant molecule from 80 to 69 Å^2. There is no systematic trend in the difference between the equilibrium and fitted interfacial tensions for the SDS concentrations we have considered. Variations of other physical parameters within their experimental uncertainties had no discernible effects on the quality of the fit to the force data. For example, using a value of -30 mV, which is at one extreme of the range for the surface potential of the silica particle, has no visible effect on the results in Figure 4.

Using the theory of Chan et al.,[1] it is possible to deduce a quantitative picture of the deformation of the droplet interface from the force vs displacement data. We will illustrate this with results for two different cases: 10^{-2}

M SDS in 10^{-3} M NaNO$_3$ and 10^{-5} M SDS in 10^{-3} M NaNO$_3$, in Figure 5. In each case, the solid lines represent the theoretical forces calculated using a fitted value of the interfacial tension (see Table 3) and assuming that the three phase contact line is immobile. For Figure 5a, the interfacial tension is 9.8 mN/m as opposed to the equilibrium value of 8.6 mN/m. For Figure 5b, the interfacial tension is 38.5 mN/m as opposed to the equilibrium value of 39.1 mN/m. Points at various values of F/a, as indicated by letters A–E in Figure 5, are chosen to facilitate discussion.

In Figure 6a, the force normalized by the particle probe radius, F/a is shown as a function of D_o, the distance of closest approach between the particle probe and the droplet (see Figure 1a). These curves are obtained from theory[1] and are labeled with the points A–E corresponding to those in Figure 5a. We note that all points A–E along the force curve correspond to a range of distances of closest approach, D_o that exceed 4 Debye screening lengths. Consequently, in terms of the electrostatic disjoining pressure between the particle and the droplet, the interaction remains in the so-called superposition regime where there is no difference between constant charge or constant potential boundary conditions. The same can also be observed for Figures 6b, although the Debye screening length is longer than that in case a, but D_o is still greater than 0.8 Debye screening lengths. In both instances, the van der Waals contribution to the disjoining pressure is negligible over the range of D_o in Figure 6. The measured force regime all corresponds to distances of closest approach, $D_o > 10$ nm, or $\kappa D_o > 0.8$ to $\kappa D_o > 4$. In this region of the scaled separation, the disjoining pressure,
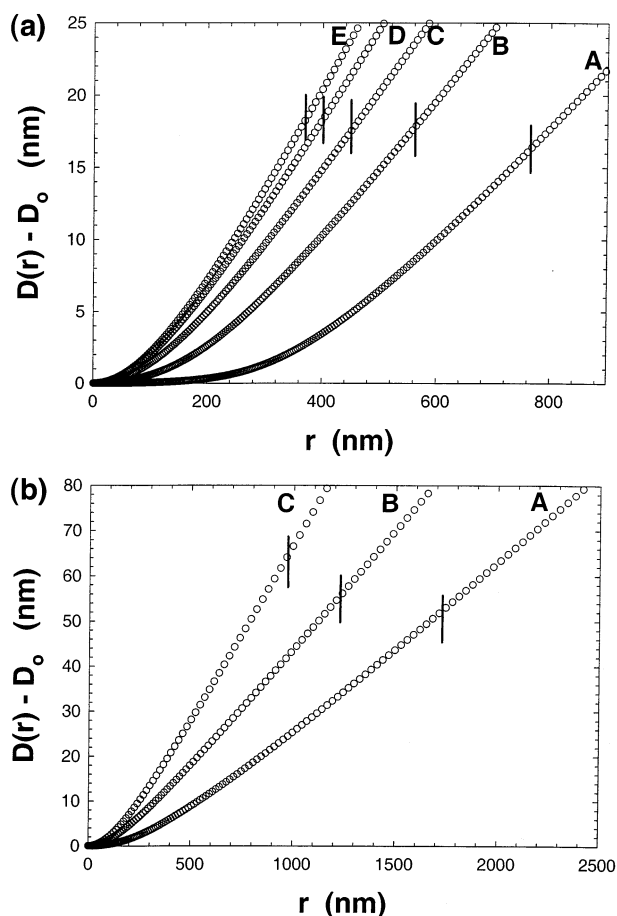
Figure 9. (a) Plot of $D(r) - D_0$ vs r. 10^{-2} M SDS, 10^{-3} M NaNO$_3$. The theoretical calculation using $\psi_{o1} = -50$ mV, $\psi_{o2} = -100$ mV, $\gamma^{\text{fitted}} = 9.8$ mN/m, $R_o = 0.5$ mm, $a = 2.16$ μm, $\theta = 92°$ and $\kappa^{-1} = 2.92$ nm. For A–E, refer to Figure 6a. The solid lines indicate the distance where greater than 95% of the total force has been accounted for by the disjoining pressure. (b) Plot of $D(r)$-D_0 vs r. 10^{-5} M SDS, 10^{-3} M NaNO$_3$. The theoretical calculation was performed using $\psi_{o1} = -50$ mV, $\psi_{o2} = -100$ mV, $\gamma^{\text{fitted}} = 38.5$ mN/m, $R_o = 0.5$ mm, $a = 2.16$ μm, $\theta = 102°$, and $\kappa^{-1} = 9.54$ nm. For A–C, refer to Figure 6b. The solid lines indicate the distance where greater than 95% of the total force has been accounted for by the disjoining pressure.

due only to electrical double layer interactions, is well approximated by an exponential function. Consequently, an independent determination of surface potentials as we have done here, is necessary to determine the distance of closest approach, D_o without ambiguities.

In all of the cases presented here, the large forces that are observed as D_o approaches D_w, are due to deformations of the droplet interface which gives rise to a larger effective areas of interaction. To see this, we note that due to the exponential form of the disjoining pressure, the minimum separation, D_w, as calculated from eq 18 is relatively insensitive to the SDS concentration or interfacial tensions (see Table 4). Therefore, the rapid increases in the force, F, as D_o approaches D_w, observed in Figure 6 must be due to increases in the effective interaction area as the droplet deforms. To quantify this observation, we show in Figure 7 the observed force divided by the force, F_{rigid}, calculated from a rigid, nondeformable droplet interface with identical electrochemical properties for the case of 10^{-2} M SDS in 10^{-3} M NaNO$_3$. Here we see that deformation of the droplet can increase the effective area of interaction by over 10-fold.

It is also instructive to examine the shape of the decane–water interface that corresponds to various points on the force curves in Figure 5.

Droplet Profile. In Figure 8, the droplet profiles, $z(r) - z_0$ (see Figure 1a for geometrical significance) deduced from theory[1] are shown corresponding to points A–E in Figures 5 and 6.

The droplet profile corresponding to the lowest interfacial tension, 10^{-2} M SDS, 10^{-3} M NaNO$_3$, is presented in Figure 8a. At large separations (cases D and E) where $D_o > 19$ nm, the fluid interface is concave down. For smaller separations (cases A–C) where $D_o < 15$ nm, the fluid interface changes curvature. Note the disparate scales on the x and y axes. To emphasize the scale difference, the sphere size and the inverse of the Debye length, κ^{-1} are indicated in Figure 8a. A magnified view of the small r region (<500 nm) is also given. In Figure 8b, droplet profiles for the case 10^{-5} M SDS in 10^{-3} M NaNO$_3$ are shown. Again, note that the convexity changes from curves A to C.

In Figure 9, parts a and b, we show $D(r) - D_o$, the distance between particle probe and the droplet interface (see Figure 1a for the geometric significance) for the cases of 10^{-2} M SDS and 10^{-5} M SDS in 10^{-3} M NaNO$_3$. The curves labeled A–E correspond to the points on the force curves introduced earlier in Figure 5. The solid vertical lines in Figure 9 indicate the radial regions in which over 95% of the total force is accounted for by the disjoining pressure acting inside these regions. These results indicate that for modest to low forces, $F/a \leq 2$ mN/m, only a relatively small fraction of the surface of the particle probe (radius 2.16 μm) is involved in the particle–droplet interface interaction.

Conclusions

In the analysis of force measurements in SDS solutions, we saw that an unambiguous determination of the absolute separation between the particle probe and the droplet interface required knowing the values of all physical parameters of the system. Using the independently determined physical parameters as input, the theoretical curves fall within experimental uncertainties of force measurements for the SDS solutions. The adsorption of SDS provides the droplet interface with a surface potential of sufficiently high magnitude to stabilize the particle–droplet system against engulfment due to the ever present attractive van der Waals interactions. Under these circumstances, deformation of the droplet interface provides a mechanism to increase the effective areas of repulsive interaction between the particle and the droplet which stabilizes the system against engulfment even at the highest forces that we can apply in the present experiment. Unlike earlier measurements (Aston and Berg), we observed no systematic variations of the force within a range of speed of approach of the piezo electric stage even at speeds above those reported by Aston and Berg where they observed speed dependent forces.[28]